Hierarchical Wide-Area Control of Power Systems Including Wind Farms and FACTS for Short-Term Frequency Regulation

Andres E. Leon, *Graduate Student Member, IEEE*, Juan Manuel Mauricio, *Member, IEEE*, Antonio Gómez-Expósito, *Fellow, IEEE*, and Jorge A. Solsona, *Senior Member, IEEE*

***Abstract*—In this work a hierarchical scheme is proposed for the coordinated control of conventional synchronous generators, wind farm converters and flexible ac transmission systems. It comprises two levels, namely a fully decentralized set of controllers associated with the involved devices and a centralized coordinating controller based on synchronized wide-area signals provided by phasor measurement units. The proposed hierarchy of controllers is mainly focused on two objectives: transient frequency support and inter-area oscillations damping. Several works have recently proved that the fast-acting power converters of variable-speed generators can greatly improve the short-term frequency regulation capability in scenarios with a large penetration of wind energy. A case study is included showing that the dynamic performance and stability of power systems can indeed be enhanced when windmill converters are properly coordinated via a wide-area centralized controller.**

***Index Terms*—Damping inter-area oscillations, FACTS devices, hierarchical controller, short-term frequency regulation, variable-speed wind generator, wide-area control.**

I. Introduction

NOWADAYS, power systems are undergoing several radical and extensive changes, such as the clear trend for generation systems to increasingly incorporate the energy coming from renewable sources, displacing as a consequence conventional fossil-fuel generators. In addition, the need to accommodate higher levels of load and remote wind-energy generation is pushing transmission lines to their stability limits, causing inter-area modes to become more lightly damped [1], [2]. Effectiveness of power system stabilizer (PSS) based approaches in damping inter-area modes is limited because such modes are not as highly controllable and observable from generator local measurements as local modes. In fact, PSS can damp inter-area modes only up to a certain transmission loading level [3]. Therefore, classical PSS structures adding damping to a local mode, and perhaps contributing also to damp an inter-area mode, may no longer be the best technical solution [1], [4].

In this context, power engineers look for solutions to enhance stability margins and control oscillatory modes by adding supplementary damping devices. Wide-area coordinating (WAC) controllers using global remote signals have been suggested since the introduction of the phasor measurement unit (PMU) technology. Remote signals transmit knowledge related to the overall network dynamics, in contrast with local signals, which often lack good observability of some significant inter-area modes [5]. Even though WAC controllers involve additional communication equipment, their implementation may turn out to be more cost effective than installing new control devices if the additional operating flexibility achieved in critical power systems compensates for the equipment cost [1], [6]. Moreover, it is expected that in future smart grids the required communication channels and PMU devices will be widely available for control purposes [7].

The WAC control approach has several challenges to overcome, such as the time delays (or latency) involved in communication systems [8]. These delays arise when remote signals are sent from PMUs to the control center through a phasor data concentrator (PDC). A global positioning system (GPS) provides precise timing pulses to correlate the signals sampled by all the PMUs [7], [9]. With present technologies, time delays are in the range of 20–500 milliseconds [10], which can deteriorate the system performance and should be considered in the control design stage [11]. Several works propose different solutions to compensate time delays in WAC controllers, for instance: a first-order Padé approximation in [1]; a strictly proper second-order Padé approximation in [10]; a Smith predictor approach in [6], [12], and [13]; a phase-shift-based technique in [14]; and a time-delay compensation based on a gain scheduling in [15], just to mention a few. Regarding the WAC control structures, diverse approaches can be found in the bibliography. LMI-based H_∞ control strategies are proposed in [6], [15], and [16]; feedback linearization procedures are established in [12], [17], and [18]; a particle swarm optimization technique is used in [19]; an interconnection and damping assignment passivity-based controller is introduced in [20]; and a neural network-based scheme is designed in [21].

Even though one of the most attractive features of the WAC control is its capability to simultaneously coordinate different

Manuscript received August 11, 2011; revised December 21, 2011; accepted February 24, 2012. Date of publication April 04, 2012; date of current version October 17, 2012. This work was supported by Universidad Nacional del Sur, Consejo Nacional de Investigaciones Científicas y Técnicas (CONICET) and Agencia Nacional de Promoción Científica y Tecnológica (ANPCyT), Argentina, and by the Spanish Ministry of Education and Science (MEC) and Junta de Andalucía under grants ENE2011-24137 and P09-TEP-5170, respectively. Paper no. TPWRS-00762-2011.

A. E. Leon and J. A. Solsona are with the Instituto de Investigaciones en Ingeniería Eléctrica (IIIE) "Alfredo Desages" (UNS-CONICET), Universidad Nacional del Sur (DIEC-UNS), 8000 Bahía Blanca, Argentina (e-mail: aleon@ymail.com; jsolsona@uns.edu.ar).

J. M. Mauricio and A. Gómez-Expósito are with the Department of Electrical Engineering, University of Seville, 41092 Seville, Spain (e-mail: j.m.mauricio@ieee.org; age@us.es).

Digital Object Identifier 10.1109/TPWRS.2012.2189419

devices such as synchronous generators (SG) and flexible alternating current transmission systems (FACTS), many previous works only analyze the control of SG (for example in references [1]–[3], [10], [11], [13], and [15]–[20]), or FACTS (for example [1], [3], [6], [14], [21], and [22]), lacking a coordinated action. The potential of WAC controllers to control SG and FACTS in a coordinated manner is explored in [5] and [12]. To the authors knowledge, there is no bibliography in which the coordinated control of SG, FACTS and wind farm power converters is thoroughly addressed.

The main contribution of this work is the inclusion of wind energy conversion systems (WECS) into WAC controllers, in a coordinated manner with other power devices, so as to improve the frequency response and stability of interconnected power systems. The goal is to exploit the quick reaction of the converters associated with variable-speed WECS, which are advantageous over SG and FACTS when fast active power injection to the grid is transiently required [23], [24]. Mechanical time constants of SG are slower than converter time constants, whereas FACTS lack the capability to inject active power unless they are accompanied by energy storage systems. Both features (speed and stored energy) are naturally found in WECS which can resort to the kinetic energy stored in the rotational masses via power electronics [25]–[27]. In this work, this objective is addressed by means of a two-level hierarchical controller, namely a fully decentralized control level and a centralized one which uses global information to add supplementary damping signals to the local controllers. The first level comprises the conventional controllers currently found in SG, FACTS, and WECS facilities, providing a stabilizing action for local modes and local voltage regulation. These primary strategies do not use global information and guarantee an acceptable performance when the WAC control is turned off due to loss of communication links. The second-level WAC controller is mainly focused on both inter-area oscillations damping and transient frequency support when sudden and noticeable active power changes occur.

The paper is organized as follows. Section II introduces the model of power system components. The first-level decentralized and second-level centralized control designs are developed in Sections III and IV, respectively. In Section V the WAC controller performance assessment, discussions, and tests are presented. Finally, conclusions are given in Section VI.

II. Power System Model

A. SG, FACTS, and WECS Description

A power system can be represented by a set of nonlinear differential-algebraic equations as follows:

$$\dot{\mathbf{x}} = \mathbf{f}(\mathbf{x}, \mathbf{z}, \mathbf{u}) \tag{1}$$

$$\mathbf{0} = \mathbf{g}(\mathbf{x}, \mathbf{z}, \mathbf{u}) \tag{2}$$

$$\mathbf{y} = \mathbf{h}(\mathbf{x}, \mathbf{z}, \mathbf{u}) \tag{3}$$

where vector $\mathbf{x}$ stands for differential states of SG, WECS, and FACTS devices, including their decentralized controllers such as governors (GOV), automatic voltage regulators (AVR), PSSs, and local controllers of WECS and FACTS. The algebraic states, for instance generator stator currents, phase angles, and amplitudes of network bus voltages, are denoted by $\mathbf{z}$. Vector $\mathbf{y}$ represents measurements or states to be fed back, whereas $\mathbf{u} = [\mathbf{u}_{sg} \quad \mathbf{u}_{wecs} \quad \mathbf{u}_{facts}]^T$ is the vector containing all the supplementary control inputs from the WAC controller. These supplementary inputs comprise a remote "voltage" signal v_{cc} added to the excitation system of synchronous generators, as well as additional active and reactive powers injected by WECS (Δp_w and Δq_w), and FACTS (Δp_f and Δq_f) (Fig. 1 shows how these signals interact with each local controller). Consequently

$$\mathbf{u}_{sg} = [\, v_{cc1} \quad \cdots \quad v_{cci} \quad \cdots \quad v_{ccn} \,]^T \tag{4}$$

$$\mathbf{u}_{wecs} = [\, \Delta p_{w1} \quad \Delta q_{w1} \quad \cdots \quad \Delta p_{wm} \quad \Delta q_{wm} \,]^T \tag{5}$$

$$\mathbf{u}_{facts} = [\, \Delta p_{f1} \quad \Delta q_{f1} \quad \cdots \quad \Delta p_{fk} \quad \Delta q_{fk} \,]^T. \tag{6}$$

In this work loads are modeled as a combination of constant impedance, current and power loads.

III. First-Level Decentralized Control

At this level, conventional control strategies are resorted to regarding the controllers and equipment in the different facilities affected by the WAC control. Accordingly, a local control scheme based on GOV-AVR-PSS devices is assumed for synchronous generators (see bottom of Fig. 1). In shunt FACTS, performing voltage regulation, classical voltage-current characteristic is used to control their injected reactive power. In WECS, the active and reactive power management and control implementation are shown at the top of Fig. 1. The active power loop consists of three terms: first, a term from a maximum power point tracking (MPPT) algorithm which, by using a lookup table of the turbine maximum power curve and measuring the turbine speed, gets the optimal active power [23]; second, a local frequency contribution based on a local frequency measurement [25]–[27]; and third, a remote signal from the WAC control (which will be explained in the next section). On the other hand, the reactive power loop consists of a low-voltage ride-through curve (which was extracted from the Spanish grid code requirements [28]). This curve gives the voltage/reactive current characteristic which determines the reactive power injection to support the voltage amplitude during sags or faults in the network [29]. The reactive control loop also has a WAC signal.

IV. Second-Level Centralized Control

The second level is built around a WAC controller, which is tuned keeping in mind the dynamics of the first-level (local) controllers (the reader is referred to Fig. 1 for the details regarding the place where the supplementary WAC signals are added to the local controllers). At this point, two remarks have to be done. Firstly, when the proposed short-term frequency regulation is performed, the maximum active power of the wind turbine is modified. However, these power variations only take place transiently in a short period of time after a load step occurs, while in steady state operation, the MPPT algorithm is followed. Consequently, power deviations from the optimal point only happen transiently during a sudden load variation or network fault, whereas most of the time the wind farm is operating at its optimal wind power generation. Therefore, the MPPT and

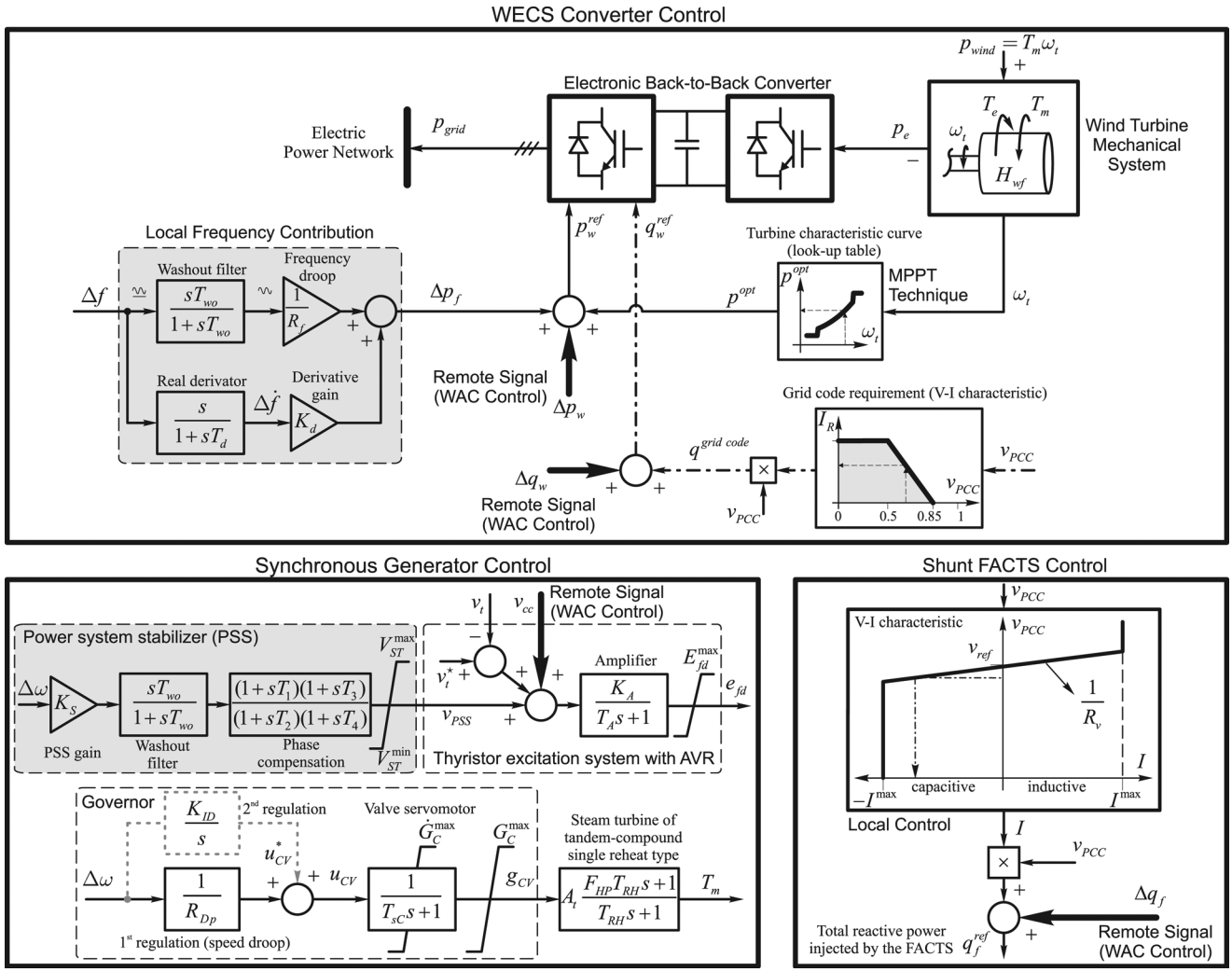

Fig. 1. Block diagram of local controllers and the place where the supplementary WAC signals are added to each device.

the proposed transient frequency regulation are not incompatible from each other. Secondly, the secondary frequency regulation is accomplished only by the governing system of synchronous generators. Since the time scale of the secondary regulation is longer than local and wide-area transient frequency support, the secondary regulation can be tuned as in a conventional power system without risk of interactions between control loops.

The design procedure of the WAC control is developed in three stages: firstly, a power system model reduction is accomplished by using a balanced model truncation, in combination with two-state transformations so that the reduced internal states become physically measured states; secondly, the system model is extended with a transmission time-delay block in order to enhance the WAC control performance against typical delays of communication channels; finally, a state feedback control law is designed based on an optimal quadratic technique to minimize the control energy of each power device.

A. Power System Reduction and Proposed Transformations

1) Power System Model for the Controller Design: Power systems usually have several hundreds or even thousands of states. As designing a controller with such a high-order model is neither practical nor necessary, a model reduction is often applied to obtain a lower-order model for the control design stage [16], such as the one summarized below.

The linearized power system model can be written as

$$\dot{\mathbf{x}}^{n\times 1} = \mathbf{A}^{n\times n}\mathbf{x}^{n\times 1} + \mathbf{B}^{n\times p}\mathbf{u}^{p\times 1} \tag{7}$$

$$\mathbf{y}^{m\times 1} = \mathbf{C}^{m\times n}\mathbf{x}^{n\times 1}. \tag{8}$$

Matrix and vector dimensions are indicated as superscripts to clarify the transformations below, where n, p, and m are the number of differential states, control inputs, and measured outputs, respectively.

Considering the system (7), (8), and using the balanced model truncation via square root method, the following reduced model is obtained:

$$\dot{\mathbf{w}}^{r\times 1} = \mathbf{S}_L^{T\ r\times n}\mathbf{A}^{n\times n}\mathbf{S}_R^{n\times r}\mathbf{w}^{r\times 1} + \mathbf{S}_L^{T\ r\times n}\mathbf{B}^{n\times p}\mathbf{u}^{p\times 1} \tag{9}$$

$$\mathbf{y}^{m\times 1} = \mathbf{C}^{m\times n}\mathbf{S}_R^{n\times r}\mathbf{w}^{r\times 1}. \tag{10}$$

Details of the reduction methodology can be found for example in [30] and [31]. States $\mathbf{w}$ represent the internal states of the reduced model (9), (10), where $r < n$ is the number of reduced

states, and $\mathbf{S}_L$ and $\mathbf{S}_R$ are appropriate matrices which allow reducing the power system model. When reduction methods are applied, although the reduced system behaves like the original one, from an input-output point of view ($\mathbf{u} \mapsto \mathbf{y}$), the reduced internal states $\mathbf{w}$ do not have physical meaning, and cannot be measured. The reduced system is useful to design input-output controllers, like PSSs or lead-lag compensators [3], [6], [10], [11], [16], [22], [31], [32]. However, when designing a high-performance input-state controller, some modifications must be considered in order to overcome the above limitation (i.e., reduced internal states without physical meaning). For this purpose, the following transformation $\mathbf{T}^{m\times r}$ is proposed:

$$\mathbf{T}^{m\times r} \triangleq \mathbf{C}^{m\times n}\mathbf{S}_R^{n\times r}. \tag{11}$$

Note that, if a number of measured states equal to the number of reduced internal states is chosen ($m = r$), then $\mathbf{T}^{m\times r}$ will be a square matrix, and according to (10) the transformation $\mathbf{w} \mapsto \mathbf{y}$ will be reliable. This transformation allows the reduced model to be written with $\mathbf{y}$ as dynamic states. Therefore, applying (11) to the system (9) yields

$$\dot{\mathbf{y}} = \mathbf{T}\mathbf{S}_L^T\mathbf{A}\mathbf{S}_R\mathbf{T}^{-1}\mathbf{y} + \mathbf{T}\mathbf{S}_L^T\mathbf{B}\mathbf{u}. \tag{12}$$

With the resulting system (12), it is possible to apply state-feedback control strategies because its dynamic states $\mathbf{y}$ have physical meaning.

2) Measurement Selection: Outputs $\mathbf{y}$ can be divided into two kinds of variables: the directly measurable ones, obtained from sensors at the power system, and the indirectly measurable ones, inferred or computed from direct measurements. More frequent indirect measurements are synchronous generator internal states (for example: the load angle δ and dq-axis transient EMFs e'_q and e'_d). A procedure to obtain these indirect measurements (generator internal states) from direct measurements (voltage and current phasors) is described in the Appendix.

On the other hand, from an economic viewpoint, it is convenient to use as few measurements as possible to obtain high damping while reducing at the same time the communication and computational burden. Several techniques to select the best states to be fed back can be found in the literature, from which the most widely used are: the residue-based measures of modal observability; the geometric measures of modal observability; and methods based on participation factors. The latter is chosen in this research, as it does not undergo scaling problems when there are measures of a widely different physical significance [3], [5], [16]. The participation factor $p_{ki} = \psi_{ik}\phi_{ki}$ gives a dimensionless measure of the association between the ith mode and the kth state [33]. It combines the kth entry of the right eigenvector $\boldsymbol{\phi}_i$ with the kth entry of the left eigenvector $\boldsymbol{\psi}_i$. Therefore, most dominant states over a certain mode of interest can be found, and used to build the measure vector $\mathbf{y}$.

B. Transmission Time Delay Compensation

When using wide-area measurements, it is important to take into account the transmission time delays in the controller design stage in order to compensate the delay and to obtain a high oscillation damping and stability margin. A strictly proper second-order Padé approximation is chosen in this research because it performs better than the classical first-order Padé approximation for longer time delays [10]. It is also considered that the total time delay introduced is the sum of measurement and control time delays ($\tau = \tau_m + \tau_c$) [12]. The time-delay transfer function is given by

$$G_{delay}(s) = e^{-\tau s} \cong \frac{6 - 2\tau s}{6 + 4\tau s + \tau^2 s^2} \tag{13}$$

the state-space realization of which is

$$\dot{\mathbf{x}}_\tau = \mathbf{A}_\tau\mathbf{x}_\tau + \mathbf{B}_\tau\mathbf{v} \tag{14}$$

$$\mathbf{u} = \mathbf{C}_\tau\mathbf{x}_\tau \tag{15}$$

where $\mathbf{v}$ is the control signal at the WAC station and $\mathbf{u}$ is the control signal which arrive at the power devices (SG, WECS, FACTS, etc.) after the time delay. A dynamic extension to include this time-delay model in the controller design is proposed. It is performed by joining the reduced model (12) with the time-delay model (14), (15), yielding

$$\dot{\mathbf{x}}_e = \begin{bmatrix} \mathbf{T}\mathbf{S}_L^T\mathbf{A}\mathbf{S}_R\mathbf{T}^{-1} & \mathbf{T}\mathbf{S}_L^T\mathbf{B}\mathbf{C}_\tau \\ \mathbf{0} & \mathbf{A}_\tau \end{bmatrix}\mathbf{x}_e + \begin{bmatrix} \mathbf{0} \\ \mathbf{B}_\tau \end{bmatrix}\mathbf{v} \tag{16}$$

where $\mathbf{x}_e = [\mathbf{y}\ \mathbf{x}_\tau]^T$ is the extended state vector to be fed back.

C. Optimal Control Gain Calculation

The control signal $\mathbf{v}$ is obtained via a state-feedback controller as follows:

$$\mathbf{v} = -\mathbf{K}\mathbf{x}_e. \tag{17}$$

To maximize the oscillation damping and minimize the control efforts, the control gain $\mathbf{K}$ is calculated based on an optimal quadratic regulator technique. The optimal control gain is obtained by minimizing the cost function $J = \int \left(\mathbf{y}^T\mathbf{Q}\mathbf{y} + \mathbf{v}^T\mathbf{R}\mathbf{v}\right) dt$. This index can be built to weigh both output deviations and control inputs through the design matrix $\mathbf{Q}$ and $\mathbf{R}$. A general block diagram showing the implementation of the proposed WAC controller is presented in Fig. 2.

V. Performance Testing

This section presents the most relevant results regarding the assessment of the proposed WAC controller. The power system configuration and data used in these tests are shown in Fig. 3. GOV-AVR-PSS parameters are taken from [33, example 12.6], whereas WECS data are from [29]. WECS local frequency contribution and WAC parameters are listed in Table I.

Three kinds of controllers are evaluated: firstly, only local control in each device (SG, FACTS, WECS) is considered, with WECS local frequency contribution inhibited. This case is denoted LC; secondly, only local control is implemented, but WECS local frequency contribution is activated (LCF case); finally, full hierarchical control with local and WAC controllers is considered (WAC case). The control inputs are $\mathbf{u} = [\Delta q_f\ \Delta p_w\ \Delta q_w\ v_{cc1}\ v_{cc2}]^T$ (see Fig. 3). The power

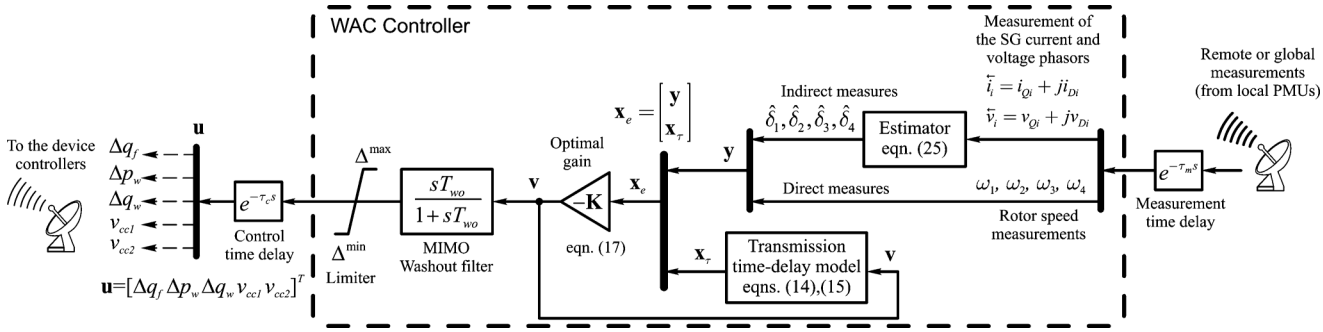

Fig. 2. Block diagram showing the implementation of the proposed WAC controller (see also Fig. 3 to get an overall picture of the control strategy).

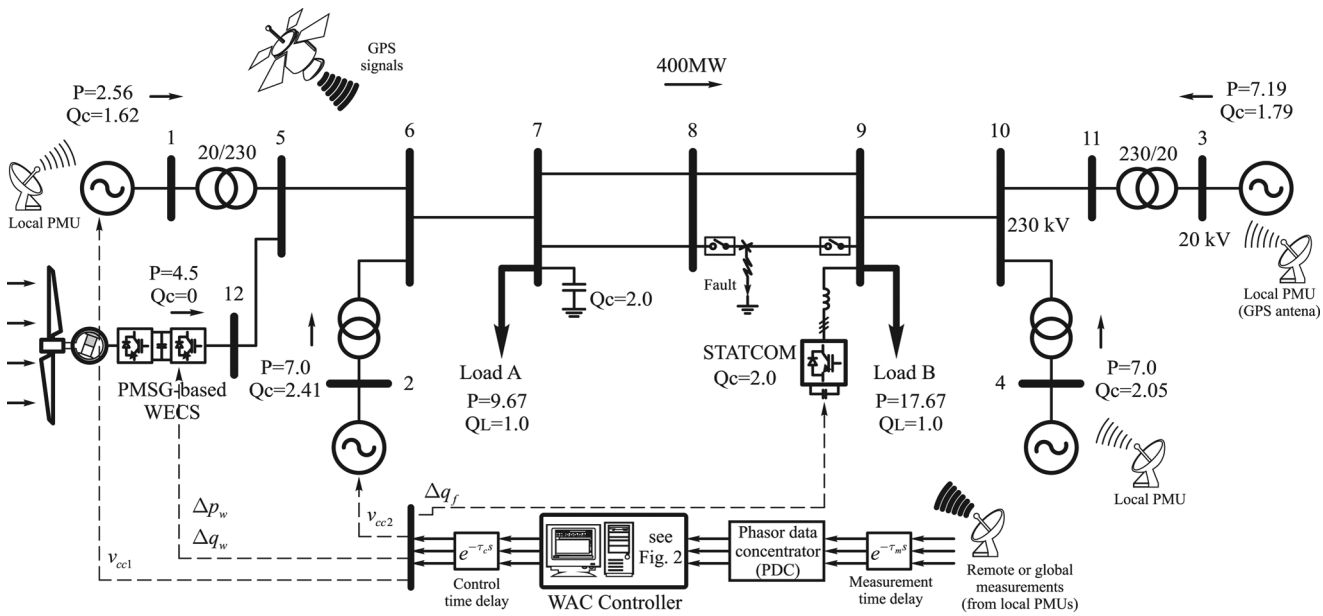

Fig. 3. Single-line diagram of the two-area five-machine study system with the WAC control (based on [33, example 12.6]).

TABLE I
CONTROL PARAMETERS

Description	Parameter	Value
Washout time const. of WECS local freq.	T_{wo}	10 s
Proportional gain of WECS local freq.	R_f	2%
Derivative time of WECS local freq.	T_d	0.04 s
Derivative gain of WECS local freq.	K_d	0.2
Total number of differential states	n	71
Number of measured and reduced states	$m = r$	8
Number of control inputs	p	5
Washout time const of WAC control	T_{wo}	5 s
Transmission time delay	τ	300 ms
WAC output limiter	Δ_{min}^{max}	$\pm$0.3 pu
Weight matrix of control inputs	$\mathbf{R}$	diag([0.3 0.5 0.5 3000 3000])
Weight matrix of output deviations	$\mathbf{Q}$	10000 diag([6 $\mathbf{I}$ 12 $\mathbf{I}$ 0.01 $\mathbf{I}$])

system and control strategy are implemented by using the SimPowerSystems blockset of MATLAB®.

A. Small-Signal Stability Analysis

The natural frequency f_n, damping ratio ζ, and participation factors for the main oscillation modes are indicated in Table II. We can see that generator load angles δ_i and rotor speeds ω_i are the states with higher participation factors in the main modes of interest. Consequently, these states are chosen to build the output vector $\mathbf{y} = [\delta_1\ \delta_2\ \delta_3\ \delta_4\ \omega_1\ \omega_2\ \omega_3\ \omega_4]^T$. Table II shows that WAC greatly improves the damping ratios when compared with the LC and LCF cases, mainly regarding the inter-area mode which increases its damping ratio to 28%, from 6% and 9%, respectively.

B. Large-Signal Stability Analysis

In this section, nonlinear time-domain simulations are carried out to assess the system-controller response to various severe disturbances.

1) Solid Three-Phase Fault Test: A 300-ms solid three-phase short circuit at bus 8 is performed, exciting all oscillatory modes of the multi-machine system. In order to assess the controller performance at various operating conditions and network topology changes, the fault is followed by an outage of one transmission line connecting buses 8 and 9 (see Fig. 3).

To show the damping of the inter-area mode, the difference between two generator load angles δ_1 and δ_3, from different areas, is depicted in Fig. 4(a). The WAC case (solid line) presents a clear improvement of the inter-area oscillation damping, when it is contrasted with the LC and LCF cases.

TABLE II
SMALL-SIGNAL STABILITY ANALYSIS

	f_n (Hz)	ζ (%)	Participation factors (%)
Local Mode #1			
LC	1.016	17.63	ω_2(23%), δ_2(23%), ω_1(20%), δ_1(18%)
LCF	1.021	16.23	ω_2(28%), δ_2(27%), ω_1(14%), δ_1(12%)
WAC	1.006	**20.61**	δ_2(20%), ω_2(18%), ω_1(6%), δ_4(6%)
Local Mode #2			
LC	1.143	15.88	ω_3(22%), ω_4(22%), δ_4(21%), δ_3(19%)
LCF	1.144	15.47	ω_3(22%), ω_4(21%), δ_4(21%), δ_3(19%)
WAC	1.287	**22.03**	ω_4(19%), δ_4(16%), e'_{q4}(13%), ω_3(10%), δ_3(7%)
Inter-area Mode			
LC	0.603	6.23	ω_3(14%), ω_4(13%), δ_3(13%), ω_1(13%), δ_4(13%)
LCF	0.569	9.41	ω_3(15%), ω_4(15%), δ_3(14%), δ_4(14%), ω_1(9%)
WAC	0.586	**27.74**	δ_3(24%), δ_4(17%), ω_3(15%), ω_4(6%), ω_1(4%)

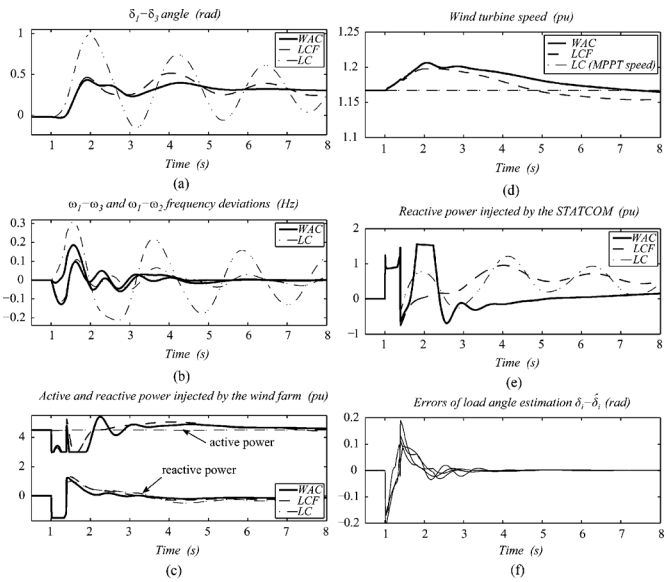

Fig. 4. System and controller behavior against a 300-ms solid three-phase short circuit at bus 8.

Differences between rotor speeds of inter- and intra-area generators are also illustrated in Fig. 4(b). As in the above plot, a better performance can be noted from the oscillation damping perspective, when the proposed WAC scheme is considered. The active and reactive powers transiently injected by the wind farm are shown in Fig. 4(c). It can be seen that power excursions are bounded to prevent excessive control action. In the transient period, the injected active power is in average lower than that received from the wind, which explains the turbine speed increase observed in Fig. 4(d). The WAC control shifts transiently the windmill speed (within an acceptable range) from the MPPT point but it returns later in the steady state. The STATCOM reactive power injected to the grid for each of the three control strategies is presented in Fig. 4(e). Finally, Fig. 4(f) shows the estimation errors of load angles (indirectly measured states) introduced by the algorithm developed in the Appendix. As can be concluded from the above results, these errors are small enough to allow increasing the oscillation damping.

2) Frequency Support Against Sudden Load Changes: In this subsection, two tests illustrate the frequency regulation capability of the proposed strategy. Firstly, a negative load step of 200 MW at bus 7 is simulated. This creates a mismatch between generation and consumption which tends to increase the system frequency. Both the WECS local frequency contribution and the proposed WAC controller attempt to reduce the transient frequency deviations in the presence of these imbalances by resorting to the kinetic energy stored in the windmill inertia. In this example, Fig. 5(a) shows the frequency response when the LC control (dash-dot line), LCF control (dashed line), and the WAC control (solid line) are implemented. When the LC strategy is used a frequency overshoot of 0.32 Hz is observed; then, when WECS local frequency contribution is included (LCF case), the frequency overshoot becomes 0.23 Hz (a reduction of 28%); finally, when the WAC control is applied an overshoot of just 0.18 Hz is obtained (a reduction of 44%). This clearly illustrates the transient improvement of the system frequency which can be brought about by wind farms when they are properly controlled by WAC strategies. The steady-state error in the system frequency is cancelled out by the governor secondary regulation at other time scale (not shown in the figure). Active and reactive powers injected to the grid by the WECS are illustrated in Fig. 5(b). Since the average active power is lower than the wind power, the wind turbine undergoes a temporary speed increase [see Fig. 5(c)].

In the second test, a positive load step of 200 MW at bus 7 is simulated (in practice this is equivalent to a loss of a generating unit). Frequency deviations, active and reactive powers injected by the wind farm, and wind turbine speeds are shown in Fig. 6. As in the previous case, similar percentage improvements can be observed when the WAC control is implemented. In this case, as the average active power is higher than the wind power, a speed reduction is transiently experienced by the wind turbine. However, the speed is again kept inside the normal variable-speed operating range of the WECS.

VI. CONCLUSIONS

A two-level hierarchical control strategy oriented for future power systems with an important amount of FACTS and wind energy conversion systems is proposed in this paper. The most relevant aspect of the wide-area coordinating controller is that it allows wind generators to contribute to frequency support and to help damp the oscillation of the most important modes.

A state feedback control law is proposed tuned through an optimal quadratic technique. To design this controller the dynamic model of the power system is reduced and a transformation is applied in order to obtain the measured outputs as dynamic states. With this approach the resulting model states keep the physical meaning of the original ones. The control strategy shows a good performance and robustness for different conditions of the power system. Several test results show a significant improvement of the power system frequency and damping response when remote signals are considered by the WAC control strategy coordinating SG, FACTS, and WECS.

APPENDIX

Some generator internal states (δ, e'_q, e'_d) are not directly measured in generating stations. Therefore, they need to be calculated using measurable quantities, such as v_D, v_Q, i_D, i_Q, being

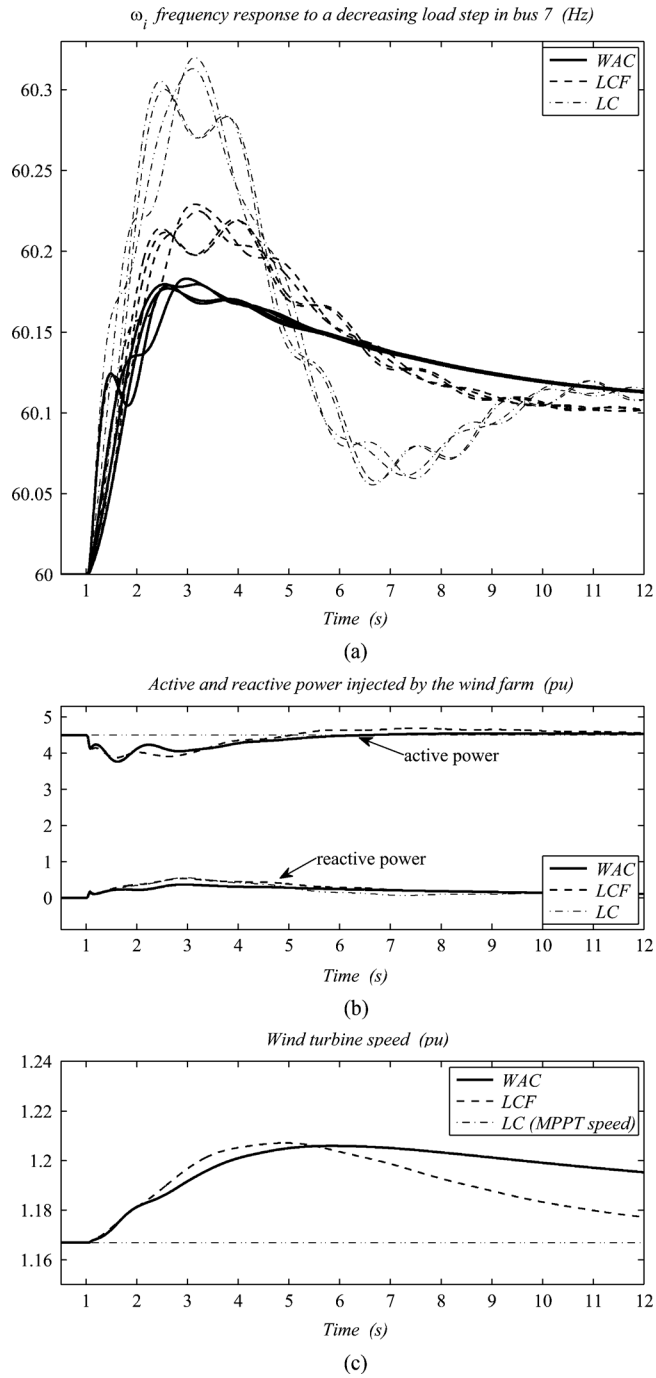

Fig. 5. Frequency and WECS responses to a -200 MW step at bus 7.

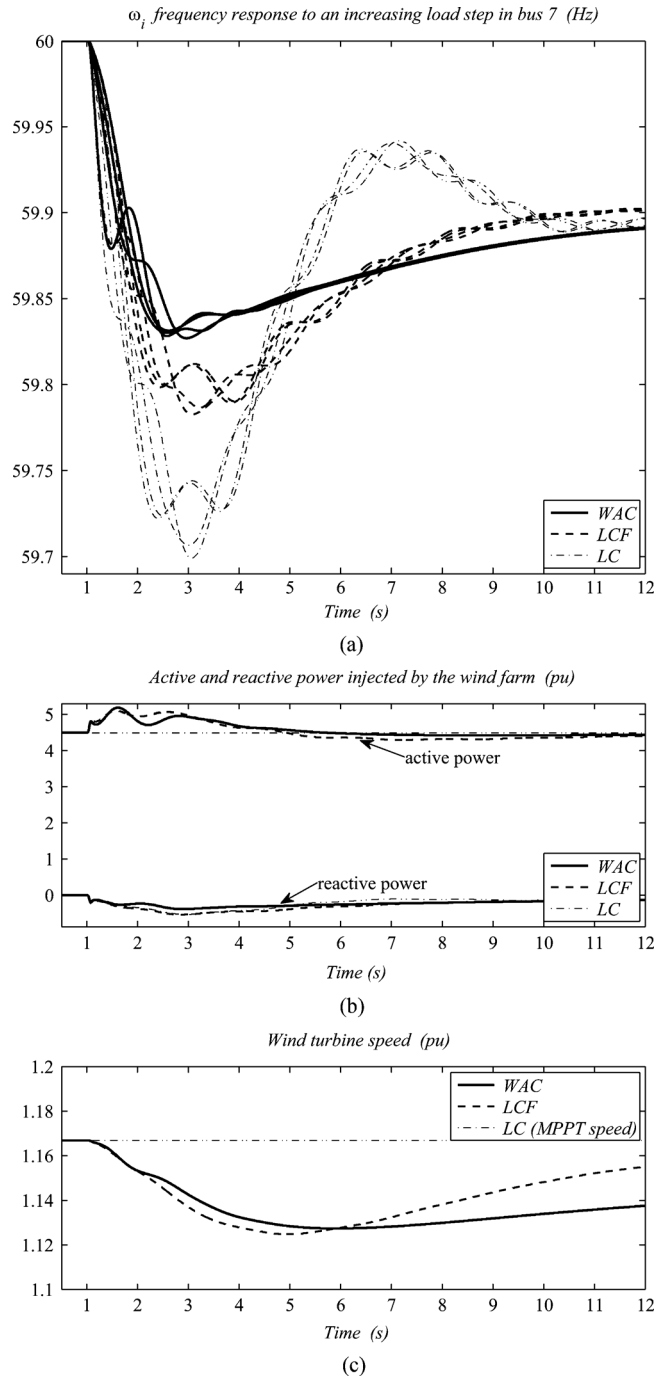

Fig. 6. Frequency and WECS responses to a $+200$ MW step at bus 7.

$v_r e^{j\theta_r} = v_Q + jv_D$ and $ie^{j(\theta_r - \phi)} = i_Q + ji_D$ the terminal generator voltage and current obtained from the local PMUs. The whole procedure is omitted owing to for space limitations, but a guideline is presented in this Appendix. Strategies using static estimations of unmeasured states, which are similar to the one introduced here, can be found in [34]–[37].

The above measured signals are expressed in the PMU synchronous DQ reference frame, and they can be related to the local dq reference frame of each generator (which rotates with its own rotor) via the following relationships:

$$v_D = v_d \cos\delta + v_q \sin\delta \tag{18}$$

$$v_Q = v_q \cos\delta - v_d \sin\delta \tag{19}$$

$$i_D = i_d \cos\delta + i_q \sin\delta \tag{20}$$

$$i_Q = i_q \cos\delta - i_d \sin\delta. \tag{21}$$

Additionally, the generator stator algebraic constraints are

$$0 = R_{sr} i_d + L'_{qr} i_q - e'_d + v_d \tag{22}$$

$$0 = R_{sr} i_q - L'_{dr} i_d - e'_q + v_q. \tag{23}$$

Assuming that $T'_{q0} \ll T'_{d0}$, which is equivalent to consider that the e'_d dynamics is faster than the e'_q dynamics, it is possible to consider that the d-axis transient EMF (e'_d) is an algebraic state

($T'_{q0} \cong 0$). Therefore, from the generator dynamic model, the following algebraic equation is obtained:

$$0 \cong e'_d + \left(L_{qr} - L'_{qr}\right) i_q. \tag{24}$$

For more details of the above generator model, see [33]. Equations (18)–(24) represent a nonlinear equation system from which, using a symbolic software, the desired unmeasured states can be obtained. Consequently, equations relating unmeasured variables to measured ones are

$$\begin{bmatrix} \hat{\delta} & \hat{e}'_q & \hat{e}'_d \end{bmatrix}^T = \begin{bmatrix} \arccos(\beta) \\ \beta\left(R_{sr} i_Q - L'_{dr} i_D + v_Q\right) + \sqrt{1-\beta^2}\left(R_{sr} i_D + L'_{dr} i_Q + v_D\right) \\ \beta\left(R_{sr} i_D + L'_{qr} i_Q + v_D\right) - \sqrt{1-\beta^2}\left(R_{sr} i_Q - L'_{qr} i_D + v_Q\right) \end{bmatrix} \tag{25}$$

where

$$\beta \triangleq \frac{R_{sr} i_Q - L_{qr} i_D + v_Q}{\sqrt{\left(R_{sr} i_D + L_{qr} i_Q + v_D\right)^2 + \left(R_{sr} i_Q - L_{qr} i_D + v_Q\right)^2}}.$$

The symbol ($\hat{}$) is used to indicate an estimated value, whereas $R_{sr}, L_{qr}, L'_{dr}, L'_{qr}$ stand for the stator resistance, q-axis inductance, and d- and q-axis transient inductances, respectively. Due to the simplified (24), the load angle δ is not exactly computed. However, as shown in Section V, this estimation is good enough to attain the damping objectives of the WAC controller [see estimation errors of load angles in Fig. 4(f)].

REFERENCES

[1] J. Chow, J. Sanchez-Gasca, H. Ren, and S. Wang, "Power system damping controller design-using multiple input signals," *IEEE Control Syst. Mag.*, vol. 20, no. 4, pp. 82–90, Aug. 2000.

[2] H. Far, H. Banakar, P. Li, C. Luo, and B.-T. Ooi, "Damping interarea oscillations by multiple modal selectivity method," *IEEE Trans. Power Syst.*, vol. 24, no. 2, pp. 766–775, May 2009.

[3] M. Aboul-Ela, A. Sallam, J. McCalley, and A. Fouad, "Damping controller design for power system oscillations using global signals," *IEEE Trans. Power Syst.*, vol. 11, no. 2, pp. 767–773, May 1996.

[4] M. Ghandhari, G. Andersson, and I. Hiskens, "Control Lyapunov functions for controllable series devices," *IEEE Trans. Power Syst.*, vol. 16, no. 4, pp. 689–694, Nov. 2001.

[5] I. Kamwa, R. Grondin, and Y. Hebert, "Wide-area measurement based stabilizing control of large power systems-a decentralized/hierarchical approach," *IEEE Trans. Power Syst.*, vol. 16, no. 1, pp. 136–153, Feb. 2001.

[6] B. Chaudhuri, R. Majumder, and B. Pal, "Wide-area measurement-based stabilizing control of power system considering signal transmission delay," *IEEE Trans. Power Syst.*, vol. 19, no. 4, pp. 1971–1979, Nov. 2004.

[7] I. C. Decker, A. S. eSilva, M. N. Agostini, F. B. Prioste, B. T. Mayer, and D. Dotta, "Experience and applications of phasor measurements to the Brazilian interconnected power system," *Eur. Trans. Elect. Power*, pp. 1–17, 2010.

[8] J. Stahlhut, T. Browne, G. Heydt, and V. Vittal, "Latency viewed as a stochastic process and its impact on wide area power system control signals," *IEEE Trans. Power Syst.*, vol. 23, no. 1, pp. 84–91, Feb. 2008.

[9] C. Taylor, D. Erickson, K. Martin, R. Wilson, and V. Venkatasubramanian, "WACS-wide-area stability and voltage control system: R&D and online demonstration," *Proc. IEEE*, vol. 93, no. 5, pp. 892–906, May 2005.

[10] D. Dotta, A. eSilva, and I. Decker, "Wide-area measurements-based two-level control design considering signal transmission delay," *IEEE Trans. Power Syst.*, vol. 24, no. 1, pp. 208–216, Feb. 2009.

[11] W. Yao, L. Jiang, Q. Wu, J. Wen, and S. Cheng, "Delay-dependent stability analysis of the power system with a wide-area damping controller embedded," *IEEE Trans. Power Syst.*, vol. 26, no. 1, pp. 233–240, Feb. 2011.

[12] T. Zabaiou, L.-A. Dessaint, F.-A. Okou, and R. Grondin, "Wide-area coordinating control of SVCs and synchronous generators with signal transmission delay compensation," in *Proc. IEEE Power and Energy Society General Meeting*, 2010, pp. 1–9.

[13] T. Zabaiou, F. Okou, L.-A. Dessaint, and O. Akhrif, "Time-delay compensation of a wide-area measurements-based hierarchical voltage and speed regulator," *Can. J. Elect. Comput. Eng.*, vol. 33, no. 2, pp. 77–85, 2008.

[14] N. Chaudhuri, S. Ray, R. Majumder, and B. Chaudhuri, "A new approach to continuous latency compensation with adaptive phasor power oscillation damping controller (POD)," *IEEE Trans. Power Syst.*, vol. 25, no. 2, pp. 939–946, May 2010.

[15] H. Wu, K. Tsakalis, and G. Heydt, "Evaluation of time delay effects to wide-area power system stabilizer design," *IEEE Trans. Power Syst.*, vol. 19, no. 4, pp. 1935–1941, Nov. 2004.

[16] Y. Zhang and A. Bose, "Design of wide-area damping controllers for interarea oscillations," *IEEE Trans. Power Syst.*, vol. 23, no. 3, pp. 1136–1143, Aug. 2008.

[17] S. Jain, F. Khorrami, and B. Fardanesh, "Adaptive nonlinear excitation control of power systems with unknown interconnections," *IEEE Trans. Control Syst. Technol.*, vol. 2, no. 4, pp. 436–446, Dec. 1994.

[18] F. Okou, L.-A. Dessaint, and O. Akhrif, "Power systems stability enhancement using a wide-area signals based hierarchical controller," *IEEE Trans. Power Syst.*, vol. 20, no. 3, pp. 1465–1477, Aug. 2005.

[19] P. Mitra and G. Venayagamoorthy, "Wide area control for improving stability of a power system with plug-in electric vehicles," *IET Gen., Transm. Distrib.*, vol. 4, no. 10, pp. 1151–1163, Oct. 2010.

[20] R. Ortega, M. Galaz, A. Astolfi, Y. Sun, and T. Shen, "Transient stabilization of multimachine power systems with nontrivial transfer conductances," *IEEE Trans. Autom. Control*, vol. 50, no. 1, pp. 60–75, Jan. 2005.

[21] S. Ray and G. Venayagamoorthy, "Wide-area signal-based optimal neurocontroller for a UPFC," *IEEE Trans. Power Del.*, vol. 23, no. 3, pp. 1597–1605, Jul. 2008.

[22] J. Sanchez-Gasca, "Coordinated control of two FACTS devices for damping interarea oscillations," *IEEE Trans. Power Syst.*, vol. 13, no. 2, pp. 428–434, May 1998.

[23] R. Pena, J. ClareG, and Asher, "Doubly fed induction generator using back-to-back PWM converters and its application to variable-speed wind-energy generation," *Proc. Inst. Elect. Eng., Elect. Power Appl.*, vol. 143, no. 3, pp. 231–241, May 1996.

[24] J. M. Mauricio, A. E. Leon, A. Gomez-Exposito, and J. A. Solsona, "An adaptive nonlinear controller for DFIM-based wind energy conversion systems," *IEEE Trans. Energy Convers.*, vol. 23, no. 4, pp. 1025–1035, Dec. 2008.

[25] O. Anaya-Lara, F. Hughes, N. Jenkins, and G. Strbac, "Contribution of DFIG-based wind farms to power system short-term frequency regulation," *Proc. Inst. Elect. Eng., Gen., Transm., Distrib.*, vol. 153, no. 2, pp. 164–170, 2006.

[26] J. Mauricio, A. Marano, A. Gomez-Exposito, and J. MartinezRamos, "Frequency regulation contribution through variable-speed wind energy conversion systems," *IEEE Trans. Power Syst.*, vol. 24, no. 1, pp. 173–180, Feb. 2009.

[27] D. Gautam, L. Goel, R. Ayyanar, V. Vittal, and T. Harbour, "Control strategy to mitigate the impact of reduced inertia due to doubly fed induction generators on large power systems," *IEEE Trans. Power Syst.*, vol. 26, no. 1, pp. 214–224, Feb. 2011.

[28] Red Eléctrica, P.O. 12.3, Requirements of the Response Against Voltage Sags by Special Regime Generation Assets (in Spanish), Spanish Ministry of Industry Tourism and Commerce, BOE Núm. 254, Oct. 2006. [Online]. Available: http://www.ree.es.

[29] A. E. Leon, J. M. Mauricio, A. Gomez-Exposito, and J. A. Solsona, "An improved control strategy for hybrid wind farms," *IEEE Trans. Sustain. Energy*, vol. 1, no. 3, pp. 131–141, Oct. 2010.

[30] M. Safonov and R. Chiang, "A Schur method for balanced-truncation model reduction," *IEEE Trans. Autom. Control*, vol. 34, no. 7, pp. 729–733, Jul. 1989.

[31] J. Sanchez-Gasca and J. Chow, "Power system reduction to simplify the design of damping controllers for interarea oscillations," *IEEE Trans. Power Syst.*, vol. 11, no. 3, pp. 1342–1349, Aug. 1996.

[32] E. Larsen, J. Sanchez-Gasca, and J. Chow, "Concepts for design of FACTS controllers to damp power swings," *IEEE Trans. Power Syst.*, vol. 10, no. 2, pp. 948–956, May 1995.
[33] P. Kundur, *Power System Stability and Control*. New York: McGraw-Hill, 1994.
[34] L. Fan and A. Feliachi, "Decentralized stabilization of nonlinear electric power systems using local measurements and feedback linearization," in *Proc. 43rd IEEE Midwest Symp. Circuits and Systems*, Aug. 2000, vol. 2, pp. 638–641.
[35] Q. Lu, S. Mei, W. Hu, F. F. Wu, Y. Ni, and T. Shen, "Nonlinear decentralized disturbance attenuation excitation control via new recursive design for multi-machine power systems," *IEEE Trans. Power Syst.*, vol. 16, no. 4, pp. 729–736, Nov. 2001.
[36] G. Damm, R. Marino, and F. Lamnabhi-Lagarrigue, "Adaptive nonlinear output feedback for transient stabilization and voltage regulation of power generators with unknown parameters," *Int. J. Robust Nonlin. Control*, vol. 14, no. 9-10, pp. 833–855, Jun. 2004.
[37] A. Karimi, A. Al-Hinai, K. Schoder, and A. Feliachi, "Power system stability enhancement using backstepping controller tuned by particle swarm optimization technique," in *Proc. IEEE Power Engineering Society General Meeting*, Jun. 2005, vol. 2, pp. 1388–1395.

Andres E. Leon (S'05) was born in Argentina in 1979. He received the electrical engineering degree from the Universidad Nacional del Comahue, Neuquén, Argentina, and the Ph.D. degree from the Universidad Nacional del Sur, Bahía Blanca, Argentina, in 2005 and 2011, respectively.

He is currently working at the Instituto de Investigaciones en Ingeniería Eléctrica "Alfredo Desages" (IIIE-CONICET), Bahía Blanca, Argentina. His primary areas of interest are power system control, custom power systems, and wind energy conversion systems.

Juan Manuel Mauricio (M'08) was born in Argentina in 1977. He received the electrical engineering degree from the National University of Comahue, Neuquén, Argentina, in 2003 and the M.Eng. and Ph.D. degrees from the University of Seville, Seville, Spain, in 2007 and 2009, respectively.

Since 2004, he has been with the Department of Electrical Engineering, University of Seville, where he is currently an Assistant Professor. His primary areas of interest are power systems and electrical machines modeling and control, renewable energy generation, voltage source converters-based applications, and electrical vehicles.

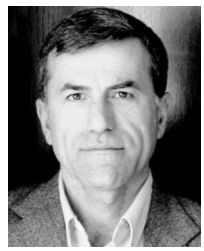

Antonio Gómez-Expósito (F'05) received the electrical engineering and Ph.D. degrees from the University of Seville, Seville, Spain.

Since 1982, he has been with the Department of Electrical Engineering, University of Seville, where he is currently a Professor and Chairman of the department. He is also directing the recently created Endesa Red Chair. His primary areas of interest are optimal power system operation, state estimation, digital signal processing, and control of flexible ac transmission system devices.

Jorge A. Solsona (SM'04) received the electronics engineer and Dr. degrees from the Universidad Nacional de La Plata, La Plata, Argentina, in 1986 and 1995, respectively.

Currently, he is with the Instituto de Investigaciones en Ingeniería Eléctrica Alfredo Desages (IIIE), Departamento de Ingeniería Eléctrica y de Computadoras, Universidad Nacional del Sur, Bahía Blanca, Argentina, and CONICET where he is involved in teaching and research on control theory and its applications to electromechanical systems.